Interferometric measurement of the temperature coefficient of the refractive index *dn/dT* and the coefficient of thermal expansion of Pr:YLF laser crystals

Orestis S. Kazasidis* and Ulrich Wittrock
Photonics Laboratory, Münster University of Applied Sciences
Stegerwaldstrasse 39, 48565 Steinfurt, Germany
*kazasidis@fh-muenster.de

Abstract: We report interferometric measurements of the temperature coefficient of the refractive index (dn/dT) and the coefficient of thermal expansion (α) of a praseodymium-doped yttrium lithium fluoride (Pr:YLF) crystal and of a fused silica reference sample. Our phase-resolved interferometric method yields a large number of data points and thus allows a precise measurement and a good error estimation. Furthermore, both dn/dT and α are obtained simultaneously from a single measurement which reduces errors that can occur in separate measurements. Over the temperature range from 20 °C to 80 °C, the value of dn/dT of Pr:YLF decreases from -5.2×10^{-6}/K to -6.2×10^{-6}/K for the ordinary refractive index and from -7.6×10^{-6}/K to -8.6×10^{-6}/K for the extraordinary refractive index. The coefficient of thermal expansion for the a-axis of Pr:YLF increases from 16.4 $\times10^{-6}$/K to 17.8 $\times10^{-6}$/K over the same temperature range.

OCIS codes: (140.3380) Laser materials; (160.5690) Rare-earth-doped materials; (160.4760) Optical properties.

References and links

1. J. L. Doualan and R. Moncorgé, "Laser crystals with low phonon frequencies," Ann. Chim. Sci. Mat. **28**, 5 – 20 (2003).
2. L. Esterowitz, R. Allen, M. Kruer, F. Bartoli, L. S. Goldberg, H. P. Jenssen, A. Linz, and V. O. Nicolai, "Blue light emission by a Pr:$LiYF_4$-laser operated at room temperature," J. Appl. Phys. **48**, 650–652 (1977).
3. T. Gün, P. Metz, and G. Huber, "Efficient continuous wave deep ultraviolet Pr^{3+}:$LiYF_4$ laser at 261.3 nm," Appl. Phys. Lett. **99**, 181103 (2011).
4. T. Sandrock, T. Danger, E. Heumann, G. Huber, and B. Chai, "Efficient continuous wave-laser emission of Pr^{3+}-doped fluorides at room temperature," Appl. Phys. B **58**, 149–151 (1994).
5. A. Richter, E. Heumann, G. Huber, V. Ostroumov, and W. Seelert, "Power scaling of semiconductor laser pumped Praseodymium-lasers," Opt. Express **15**, 5172–5178 (2007).
6. Z. Liu, Z. Cai, S. Huang, C. Zeng, Z. Meng, Y. Bu, Z. Luo, B. Xu, H. Xu, C. Ye, F. Stareki, P. Camy, and R. Moncorgé, "Diode-pumped Pr^{3+}:$LiYF_4$ continuous-wave deep red laser at 698 nm," J. Opt. Soc. Am. B **30**, 302–305 (2013).
7. P. W. Metz, F. Reichert, F. Moglia, S. Müller, D.-T. Marzahl, C. Kränkel, and G. Huber, "High-power red, orange, and green Pr^{3+}:$LiYF_4$ lasers," Opt. Lett. **39**, 3193–3196 (2014).
8. W. Koechner, *Solid State Laser Engineering* (Springer, 2006), 6th ed.

#220410 - $15.00 USD Received 4 Aug 2014; revised 7 Nov 2014; accepted 10 Nov 2014; published 3 Dec 2014

9. M. Bass, *Handbook of Optics* (McGraw-Hill, 1995).
10. CASTECH Inc, Ruanjian Avenue 89, Fuzhou, Fujian 350003, China.
11. Laser Components GmbH, Werner-von-Siemens-Str. 15, 82140 Olching, Germany.
12. N. P. Barnes and D. J. Gettemy, "Temperature variation of the refractive indices of yttrium lithium fluoride," J. Opt. Soc. Am. **70**, 1244–1247 (1980).
13. R. L. Aggarwal, D. J. Ripin, J. R. Ochoa, and T. Y. Fan, "Measurement of thermo-optic properties of $Y_3Al_5O_{12}$, $Lu_3Al_5O_{12}$, $YAlO_3$, $LiYF_4$, $LiLuF_4$, BaY_2F_8, $KGd(WO_4)_2$, and $KY(WO_4)_2$ laser crystals in the 80–300 K temperature range," J. Appl. Phys. **98**, 103514 (2005).
14. D. V. Strekalov, R. J. Thompson, L. M. Baumgartel, I. S. Grudinin, and N. Yu, "Temperature measurement and stabilization in a birefringent whispering gallery mode resonator," Opt. Express **19**, 14495–14501 (2011).
15. I. H. Malitson, "Interspecimen comparison of the refractive index of fused silica," J. Opt. Soc. Am. **55**, 1205–1208 (1965).
16. J. H. Wray and J. T. Neu, "Refractive index of several glasses as a function of wavelength and temperature," J. Opt. Soc. Am. **59**, 774–776 (1969).
17. T. Y. Fan and J. L. Daneu, "Thermal coefficients of the optical path length and refractive index in YAG," Appl. Opt. **37**, 1635–1637 (1998).
18. P.-E. Dupouy, M. Büchner, P. Paquier, G. Trénec, and J. Vigué, "Interferometric measurement of the temperature dependence of an index of refraction: application to fused silica," Appl. Opt. **49**, 678–682 (2010).
19. T. Baak, "Thermal coefficient of refractive index of optical glasses," J. Opt. Soc. Am. **59**, 851–856 (1969).
20. C. J. Parker and W. A. Popov, "Experimental determination of the effect of temperature on refractive index and optical path length of glass," Appl. Opt. **10**, 2137–2143 (1971).
21. T. S. Aurora, S. M. Day, V. King, and D. O. Pederson, "High-temperature laser interferometer for thermal expansion and optical-length measurements," Rev. Sci. Instrum. **55**, 149–152 (1984).
22. V. Cardinali, E. Marmois, B. L. Garrec, and G. Bourdet, "Determination of the thermo-optic coefficient dn/dt of ytterbium doped ceramics (Sc_2O_3, Y_2O_3, Lu_2O_3, YAG), crystals (YAG, CaF_2) and neodymium doped phosphate glass at cryogenic temperature," Opt. Mater. **34**, 990 – 994 (2012). 6th Laser Ceramics Symposium.
23. N. Ter-Gabrielyan, V. Fromzel, and M. Dubinskii, "Linear thermal expansion and thermo-optic coefficients of YVO_4 crystals the 80–320 K temperature range," Opt. Mater. Express **2**, 1624–1631 (2012).
24. Y. Sato and T. Taira, "Highly accurate interferometric evaluation of thermal expansion and dn/dt of optical materials," Opt. Mater. Express **4**, 876–888 (2014).
25. J. D. Foster and L. M. Osterink, "Index of refraction and expansion thermal coefficients of Nd:YAG," Appl. Opt. **7**, 2428–2429 (1968).
26. R. Waxler, G. Cleek, I. Malitson, M. Dodge, and T. Hahn, "Optical and mechanical properties of some neodymium-doped laser glasses," J. Res. Natl. Bur. Stand. Sec. A **75A**, 163–174 (1971).
27. T. Izumitani and H. Toratani, "Temperature coefficient of electronic polarizability in optical glasses," J. Non-Cryst. Solids **40**, 611 – 619 (1980). Proceedings of the Fifth University Conference on Glass Science.
28. J. M. Jewell, C. Askins, and I. D. Aggarwal, "Interferometric method for concurrent measurement of thermo-optic and thermal expansion coefficients," Appl. Opt. **30**, 3656–3660 (1991).
29. C. Büdenbender, "Entwicklung eines neuen Messverfahrens zur Bestimmung von thermo-optischen Konstanten von Laserkristallen," Master's thesis, Photonics Laboratory, Münster University of Applied Sciences (2009).
30. Netzsch-Gerätebau GmbH.
31. Forschungsinstitut für mineralische und metallische Werkstoffe -Edelsteine/Edelmetalle- GmbH (FEE), Struthstr. 2, D-55743 Idar-Oberstein, Germany.
32. Thorlabs GmbH, Lubeck OR Dachau/Munich, Germany.
33. M. N. Polyanskiy, "Refractive index database," (2014). [Online; accessed June 2014].
34. M. Born and E. Wolf, *Principles of Optics* (Pergamon Press, 1970), 4th ed.
35. T. Toyoda and M. Yabe, "The temperature dependence of the refractive indices of fused silica and crystal quartz," J. Phys. D: Appl. Phys. **16**, L97 (1983).
36. T. M. Pollak, R. C. Folweiler, E. P. Chicklis, J. W. Baer, A. Linz, and D. Gabbe, "Properties and fabrication of crystalline fluoride materials for high power laser applications," Tech. rep. (1980).
37. T. Pollak, W. Wing, R. Grasso, E. Chicklis, and H. Jenssen, "CW laser operation of Nd:YLF," IEEE J. Quantum Electron. **18**, 159–163 (1982).
38. S. Payne, W. F. Krupke, L. K. Smith, W. L. Kway, L. DeLoach, and J. B. Tassano, "752 nm wing-pumped Cr:LiSAF laser," IEEE J. Quantum Electron. **28**, 1188–1196 (1992).

1. Introduction

The trivalent praseodymium (Pr^{3+}) is a very attractive laser ion, offering many transitions in the visible spectrum. Its most common host is the yttrium lithium fluoride crystal ($LiYF_4$, abbreviated as YLF) because it has a low effective phonon energy [1]. The first Pr:YLF laser was realized in 1977, when Esterowitz et al. reported blue light emission at room

#220410 - $15.00 USD Received 4 Aug 2014; revised 7 Nov 2014; accepted 10 Nov 2014; published 3 Dec 2014

temperature [2], making possible the direct generation of short wavelengths with solid state lasers. Laser operation of Pr:YLF has been reported at various wavelengths from the deep ultraviolet wavelength 261.3 nm by intracavity second-harmonic generation [3] up to the visible wavelength range (e.g. 523 nm, 545 nm, 604 nm, 607 nm, 640 nm, 698 nm, and 720 nm), pumped either by gas lasers [4], frequency-doubled optically pumped semiconductor lasers, or blue laser diodes [5–7]. Exact values of the temperature coefficient of the refractive index (dn/dT) and the coefficient of thermal expansion (α) are necessary in order to calculate thermal lensing and design new laser concepts. Books, e.g. [8, 9], and laser companies, e.g. [10, 11], often quote values for dn/dT of YLF or Nd:YLF from an early publication on undoped YLF from 1980 [12]. These values were obtained by measuring the absolute refractive index at room temperature and at the temperature of liquid nitrogen. The measurement thus yields average values of dn/dT over a large temperature range. In 2005, Aggarwal et al. measured dn/dT and α of undoped YLF from 80 K to 300 K [13], and this is the only published measurement until now extending to room temperature. For an air-cooled laser operating at room temperature, the temperature inside the laser crystal can be significantly above room temperature. One would, therefore, like to have material data at elevated temperatures. We measured dn/dT and α as a function of temperature for the interval from 20 °C to 80 °C.

Recently, the difference in dn/dT between the ordinary and the extraordinary refractive index of MgF_2 has been used for temperature measurements with nK resolution in whispering gallery mode resonators [14]. The difference between the two dn/dT values is 5 times larger for YLF than for MgF_2, which would translate into a 5 times stronger signal for YLF in such a measurement, rendering YLF a good material for nK-temperature measurements.

2. Experiment

Common methods to measure dn/dT of solid state materials are the prism method and the interferometric methods. In the prism method, the absolute refractive index is measured at a few discrete temperatures and dn/dT is calculated from these values [12, 15, 16]. The interferometric methods require knowledge of α in order to calculate dn/dT from the measured change in optical path length [17, 18]. Several authors performed an additional, independent measurement to obtain the required value of α [13, 19–24]. In order to increase the accuracy, some studies presented combined measurements that give both α and dn/dT [25–29]. We used the latter approach but extended it by continuously resolving the phase of the interferogram. This gives us much more data points and lets us detect changes of dn/dT with temperature over small temperature intervals. It also gives insight into statistical errors of our measurement.

2.1. Experimental setup

We measure simultaneously the change of the physical length and the change of the optical path length of a crystal as it heats up or cools down in the temperature range from 22 °C to 80 °C. In order to do so, two substrates fabricated from UV fused silica are optically contacted to two opposing surfaces of the crystal. The substrates are simply pressed onto the crystal by hand until optical contact is achieved. No adhesive is used and the crystal can be reused for other experiments. The substrates have a diameter larger than the transverse dimension of the crystal and a hole in their center which is smaller than the crystal. Figure 1 shows the assembly of the two substrates and the laser crystal. This assembly forms two Fabry-Pérot interferometers. One interferometer is formed by the gap between the inner, uncoated surfaces of the substrates and is used to measure the change of the physical length of the crystal. We call this the “substrate interferometer”. Another interferometer is formed by the two opposing surfaces of the crystal, with optical access through the holes of the substrates. This interferometer, which we call the “crystal interferometer”, is used to measure the change of the optical path length of the

#220410 - $15.00 USD Received 4 Aug 2014; revised 7 Nov 2014; accepted 10 Nov 2014; published 3 Dec 2014

crystal. The substrates have a small wedge and their outer surfaces are AR-coated in order to prevent spurious reflections. The standing waves of these two interferometers are indicated in Fig. 1 by sets of parallel green and blue lines. Approximately one fringe is visible in each interferometer due to the finite surface figure and the wedge of the crystal surfaces. The area of optical contact between the crystal and the substrates appears black, because the nearly identical indices prevent Fresnel reflection.

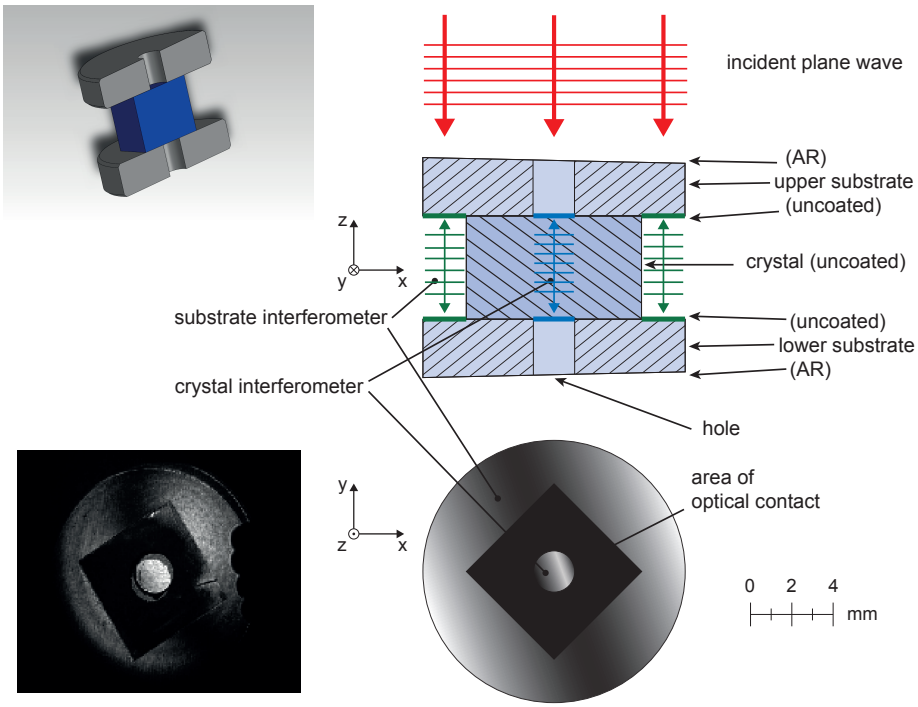

Fig. 1. In the upper left corner a 3D-cross sectional view of the assembly of the substrates and the crystal is shown, in the middle illustrations of the interferometers in a 2D-cross sectional view and in a top view are shown, and in the lower left corner a recorded interferogram is shown. The wedge angle of the substrates is exaggerated in the illustration.

The assembly of the two substrates and the crystal is placed into a vacuum chamber in order to avoid any change of the optical path length of the substrate interferometer due to changing air temperature and pressure. In the Appendix, we discuss the variation of the refractive index of the residual air in the vacuum chamber.

The complete experimental setup is shown in Fig. 2. It includes the following recording devices: a “sample” camera to record the interferograms, a “displacement” camera placed at the focal length of a lens to track any undesired angular movement of the assembly with respect to the incident laser beam, a photodiode to track power fluctuations of the laser, and two temperature sensors inside the vacuum chamber.

A linearly polarized He-Ne laser with a wavelength of 633 nm is used. The direction of the polarization can be adjusted by a half-wave plate to match the different principal axes of the Pr:YLF crystal. We checked that the beam splitters did not depolarize the beam. The beam is expanded by a telescope to a diameter slightly larger than the diameter of the substrates.

The tetragonal Pr:YLF crystal lattice has two identical a-axes and one c-axis, which is the optical axis of this uniaxial crystal. The two polished surfaces of our crystal were perpendicular

#220410 - $15.00 USD Received 4 Aug 2014; revised 7 Nov 2014; accepted 10 Nov 2014; published 3 Dec 2014

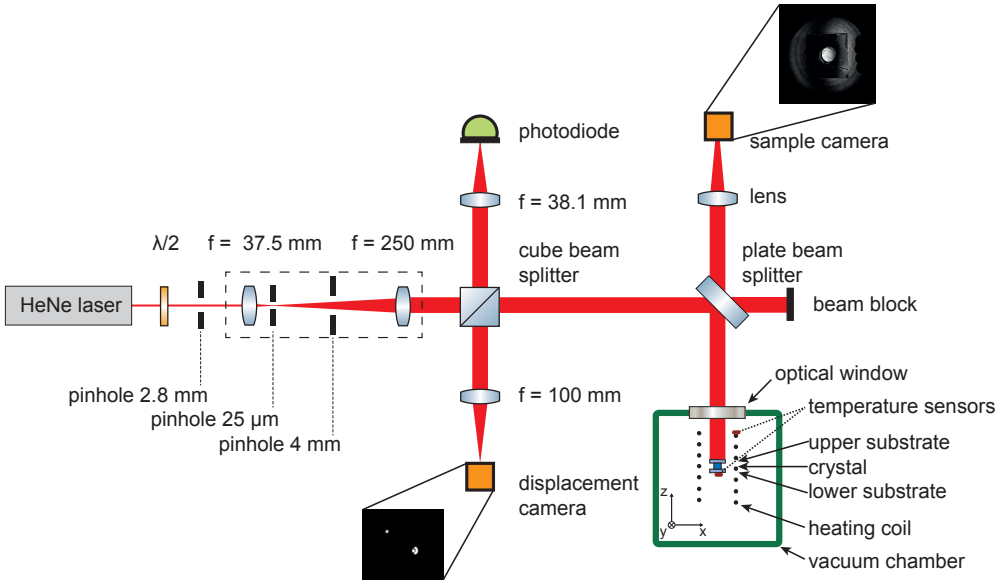

Fig. 2. The complete experimental setup and the recording devices. The dimensions of the elements and the distances between them are not to scale.

to one a-axis, which is commonly called "a-cut". Consequently, we measured the coefficient of thermal expansion (α) for the a-axis. The temperature coefficient of the refractive index (dn/dT) was measured for the ordinary polarization, i.e. light polarized parallel to the a-axis, and for the extraordinary polarization, i.e. parallel to the c-axis. In Fig. 3(a), the angle θ of the incident electric field is drawn in the crystallographic coordinate system (aac). Unless the crystal length is such that the crystal is a (multiple-order) λ-waveplate, we can find the orientation of the principal axes by a simple experiment. When θ is different from 0° or 90°, the interferogram of the crystal interferometer is a combined image of two interferograms, one from the ordinary polarization component and another from the extraordinary. This results in reduced contrast. Rotating the polarization of the incident beam changes the contrast and shifts the fringe. The fringe reverses its direction of movement when the incident light is polarized exactly parallel to the a-axis or c-axis. This allows us to determine the directions of the principal axes of the crystal. In assigning the a-axis and the c-axis to the two principal axes, we assume that the previous publications are correct and that the absolute value of dn/dT is larger for light polarized parallel to the c-axis [12]. There is another simple check to ensure that the incident beam is polarized exactly parallel to the a-axis or the c-axis: if this is not the case, a beat will be observed in the plot of the pixel intensity of the sample camera with respect to the temperature, as shown in Fig. 3(b).

Temperature control was achieved by an electrically heated coil surrounding the assembly of the substrates and the crystal. Due to the vacuum, heat was exchanged primarily by radiation. The longitudinal dimension of the coil was much larger than the height of the assembly (about 5 times) and the assembly was placed on a Teflon mount, approximately in the middle of the coil. In this way, we can assume uniform heating of the crystal. During the experiment, we varied the temperature from 22 °C to 80 °C with a 0.1 °C nominal step. For each step, the temperature of both the coil and the sample were measured at a rate of 1 Hz with the temperature sensors shown in Fig. 2. We assumed that sufficient thermalization was achieved when the standard

#220410 - $15.00 USD Received 4 Aug 2014; revised 7 Nov 2014; accepted 10 Nov 2014; published 3 Dec 2014

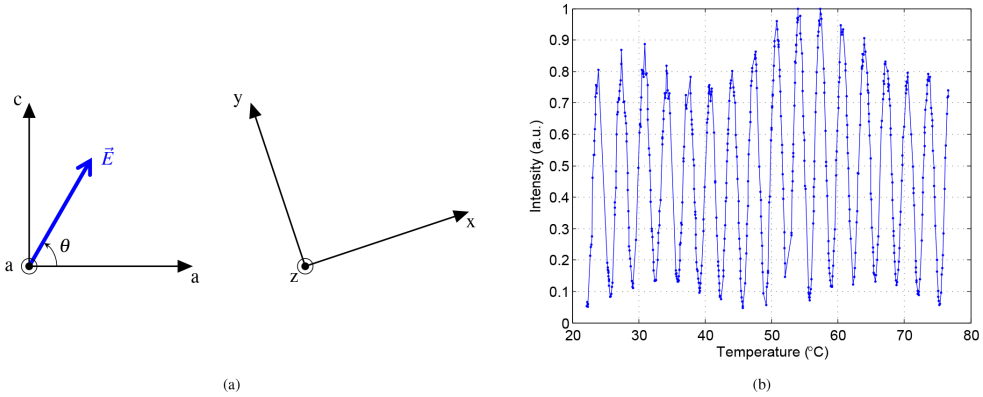

Fig. 3. (a): The electric field of the incident laser beam projected onto the crystallographic coordinate system of Pr:YLF (left) and the coordinate system defined by the mount of the crystal (right, see also Fig. 1).
(b): An example of what happens for an angle $\theta \approx 15°$. A beat is observed in the intensity variation of the crystal interferometer as the temperature is changed. The data points are connected by a continuous line for illustration purposes. Compare with Fig. 4 for a plot that occurs when the crystal is correctly aligned.

deviation of the last 20 temperature measurements of both sensors is less than 0.02 K. Once thermalization was achieved, we recorded the data from the two cameras, averaged over 10 frames. We also recorded the data from the photodiode and the pressure sensor. The mean duration of an experiment was about 11 hours, which corresponds to a heating or cooling rate smaller than 0.1 K/min.

The setup can be characterized as a modified vacuum interferometric dilatometer. The idea of simultaneously measuring thermal expansion and change in optical path length has already been used by Foster and Osterink [25], Waxler et al. [26] and Jewell et al. [28]. A fundamental difference from their setups is that we use the crystal as it is, without requiring special processing or drilling holes into it. Our method was first implemented by Büdenbender [29]. The final state of our setup resembles to the one used in the study by Izumitani and Toratani [27], which came to our knowledge during the preparation of this paper. Their publication gives little information about experimental details. One important difference to our method is that they evaluated the interferograms using only fringe counting, while we performed a phase-sensitive evaluation.

2.2. *Samples*

In order to test the setup with a well-known material we ran a preliminary series of measurements with a fused silica calibration sample manufactured by Netzsch [30]. The dimensions and the refractive index of this sample are given in Table 1. The Pr:YLF crystal that was measured was grown by FEE [31]. It was uncoated, the doping concentration was 0.42 at% and its dimensions and refractive indices are also given in Table 1.

The substrates were made of UV fused silica and manufactured by Thorlabs (type BSF10-A) [32]. They have a diameter of 12.7 mm, a center thickness of 3 mm, a wedge angle of (30 ± 10) arcmin and a single-side AR-coating for the wavelength range 350 nm - 700 nm. We bored holes of 4 mm diameter into the substrates for use with the fused silica sample, and holes of 2 mm diameter for use with the Pr:YLF crystal.

Both the substrate interferometer and the crystal interferometer are set up by the pure

#220410 - $15.00 USD Received 4 Aug 2014; revised 7 Nov 2014; accepted 10 Nov 2014; published 3 Dec 2014

Fresnel reflectivity of the uncoated surfaces, which leads to two low-finesse interferometers. The refractive indices given in Table 1 were interpolated for a wavelength of 633 nm using Sellmeier equations valid for room temperature. The Sellmeier coefficients for fused silica are from [15] and the ones for Pr:YLF are from a measurement of undoped YLF which is cited by Barnes and Gettemy as a private communication [12]. These values agree with the common literature (e.g. [33]).

Table 1: The measured samples.

Sample	***Dimensions***	***Doping***	***Refractive Index***	
			n_o	n_{eo}
Fused silica	$\varnothing$ 6 mm, $L_0 = 12$ mm	-	1.45701	
Pr:YLF	6×6 mm, $L_0 = 5$ mm	0.42 at%	1.45275	1.47534

2.3. Method

The intensity reflected from a Fabry-Pérot interferometer in the case of perpendicular incidence is [34]:

$$I_r = \frac{I_{min} + F \sin^2(\phi/2)}{1 + F \sin^2(\phi/2)} \ . \tag{1}$$

In our case of low-finesse interferometers, Eq. (1) can be simplified:

$$I_r \approx I_{min} + F \sin^2(\phi/2) = I_{min} + \frac{F}{2}(1 - \cos\phi) \ . \tag{2}$$

In the above equations I_{min} is the minimum intensity of the interferogram, which is zero for perfectly identical reflectivities of the two surfaces of the interferometer, F is the coefficient of finesse defined by the formula $F = 4R \cdot (1-R)^{-2}$ with R being the common reflectivity of the two surfaces of the interferometer, and ϕ is the phase difference of the waves reflected by the two surfaces of the interferometer:

$$\phi(T) = \frac{4\pi}{\lambda_0}\left[n(T) \cdot L(T)\right] \ , \tag{3}$$

where λ_0 is the vacuum wavelength of the light. $n(T)$ is the refractive index, $L(T)$ is the physical length, and they both depend on the temperature. Consequently, $\phi(T)$ is a function of temperature.

The coefficient of thermal expansion (α) and the temperature coefficient of the optical path length (γ) of the crystal are defined as follows:

$$\alpha = \frac{1}{L_0}\frac{dL}{dT} \ , \tag{4}$$

$$\gamma = \frac{1}{n_0 L_0}\frac{d(nL)}{dT} \ , \tag{5}$$

with n_0 and L_0 being the refractive index and the physical length of the crystal at room temperature. The temperature coefficient of the refractive index can then be calculated as:

$$\frac{dn}{dT} = n_0(\gamma - \alpha) \ . \tag{6}$$

#220410 - $15.00 USD Received 4 Aug 2014; revised 7 Nov 2014; accepted 10 Nov 2014; published 3 Dec 2014

For the case of our a-cut Pr:YLF crystal, we have the following equations for light polarized parallel to the a-axis (ordinary ray, *o*) and for light polarized parallel to the c-axis (extraordinary ray, *eo*) respectively:

$$\frac{dn_o}{dT} = n_{o,0}(\gamma_o - \alpha_a) \ , \tag{7}$$

$$\frac{dn_{eo}}{dT} = n_{eo,0}(\gamma_{eo} - \alpha_a) \ , \tag{8}$$

For the evaluation, we arbitrarily choose 100 camera pixels from the interferogram of the crystal interferometer and 100 pixels from the substrate interferogram as recorded by the sample camera. We track the phase ϕ of the intensity variation of these pixels as a function of the temperature in order to measure α and γ. This gives us many more data points than we would have by only counting fringes.

Equation (2) allows us to approximate the data for each pixel by a trigonometric function with varying frequency. We describe both the physical length (L) and the optical path length ($n \cdot L$) of the crystal using second-degree polynomials of the temperature. Consequently, the phase ϕ of the intensity variation for both interferograms, defined in Eq. (3), becomes a second-degree polynomial of the temperature, as well:

$$\phi = f_2 T^2 + f_1 T + f_0 \ , \tag{9}$$

where f_2, f_1 and f_0 are the polynomial coefficients of a fit to the experimental data. A different fit is used for each interferogram. Using Eqs. (4) and (5), both α and γ become first-degree polynomials of the temperature. From Eq. (6) it follows that dn/dT becomes a first-degree polynomial of the temperature, as well. The use of first-degree polynomials describes linear changes of α and dn/dT with temperature and is appropriate because our temperature range was only extending from 22 °C to 80 °C.

Figure 4 presents data from the two interferometers for the Pr:YLF crystal with respect to temperature together with the fitted curves. The correlation coefficient for the fit (R_{corr}) is above 0.95 for both interferometers. The strongest deviation between the fit and the data points occurs at the maxima of the intensity modulation. This variation of the maxima stimulated tracking the laser power using the photodiode. However, the variation of the maxima is not explained by the relatively small variation of the laser power, for which we subsequently corrected the data (also the data shown in Fig. 4). Since the amplitude of the intensity modulation has very small effect on the phase, this is not a serious concern.

3. Results and discussion

Using the method described in Section 2.3, we find a fit for each of the 100 pixels of the two interferometers. The mean value of all fits with $R_{corr} > 0.9$ is used to derive the coefficients α and γ. In this Section we report the resulting polynomials for α and dn/dT as a function of temperature for fused silica and Pr:YLF.

For each sample we ran several experiments, occasionally even breaking the vacuum in between and establishing new optical contact between the substrates and the crystal. The minimum temperature of our measurement interval varied between 20 °C and 23 °C and the maximum temperature varied between 75 °C and 78 °C. This was due to the automatic temperature control of the experiment and variations in laboratory temperature. We, therefore, extrapolated all results to the temperature range from 20 °C to 80 °C for direct comparison. Having data for both heating and cooling cycles, we were able to detect hysteresis which would be an indication of a measurement error, e.g. due to insufficient thermalization. However, no hysteresis larger than the standard deviation of our measurements was detected for α and dn/dT of fused silica or Pr:YLF.

#220410 - $15.00 USD Received 4 Aug 2014; revised 7 Nov 2014; accepted 10 Nov 2014; published 3 Dec 2014

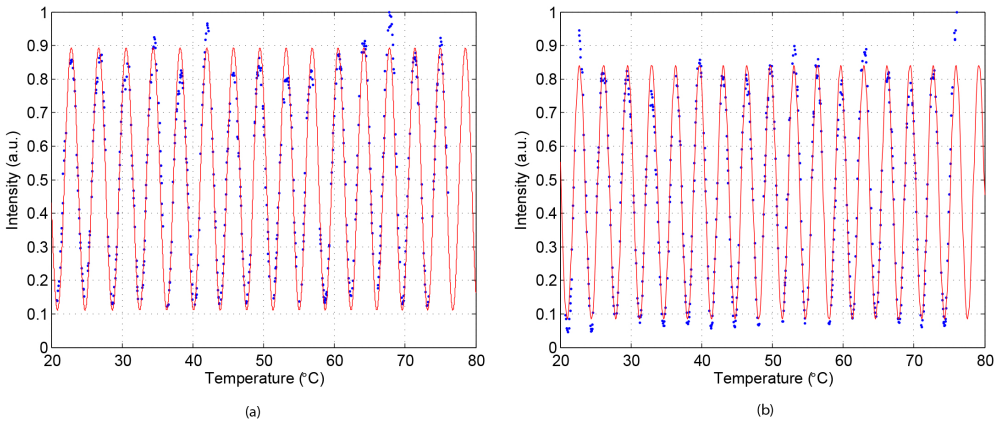

Fig. 4. Data from the interferometers for Pr:YLF together with the fitted curves. (a): The substrate interferometer, with a correlation coefficient of $R_{corr} = 0.96$. (b): The crystal interferometer, with $R_{corr} = 0.97$.

3.1. Fused silica

Fused silica is a material for which many measurements can be found in the literature. It has a relatively small coefficient of thermal expansion and, therefore, we considered it to be a good sample to test the resolution of our method. The substrate interferometer showed only one fringe for a temperature change from 20 °C to 80 °C. In order to increase the accuracy of the fit, we used Eq. (1) for the reflected intensity from a Fabry-Pérot interferometer and not the approximate Eq. (2). We also only fitted a first-degree polynomial to the physical length of the sample. We thus obtained a constant value for α for our whole temperature range. Figure 5 shows an example of the measured intensity for the substrate interferometer together with the fitted curve.

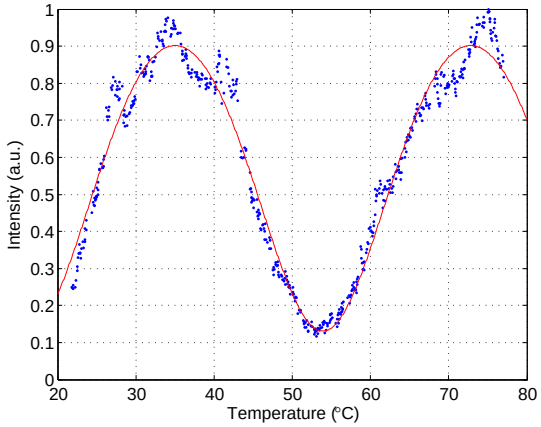

Fig. 5. An example of the measured intensity of the substrate interferometer for the fused silica sample. The fit has a correlation coefficient of $R_{corr} = 0.97$.

In the “crystal” interferometer (which of course, in these experiments, does not contain a crystal but fused silica) we detected about 24 fringes and the evaluation was made as described

#220410 - $15.00 USD Received 4 Aug 2014; revised 7 Nov 2014; accepted 10 Nov 2014; published 3 Dec 2014

in Section 2.3, meaning that we used the approximate Eq. (2) and a second degree polynomial for the optical path length.

We performed in total 13 experiments. The mean value for α is 0.64 $\times 10^{-6}$ /K. The error was estimated to be $\pm$ 0.04 $\times 10^{-6}$ /K (see Appendix). Our fused silica sample was a calibration sample for a dilatometer. From the calibration curve provided by the manufacturer we obtained an α of 0.57 $\times 10^{-6}$ /K [30], meaning that our measurement is in fairly good agreement with this value.

Using Eq. (6) the polynomial for dn/dT is:

$$\frac{dn}{dT}(T) = 0.0147 \times 10^{-6}\,\mathrm{K}^{-2} \cdot T \; + \; 5.3382 \times 10^{-6}\,\mathrm{K}^{-1} \; , \tag{10}$$

where T should be in K. The polynomial is valid for the temperature range from 20 °C to 80 °C and for a wavelength of 633 nm. The error was estimated to be $\pm$ 0.2 $\times 10^{-6}$ /K (see Appendix).

Using the prism method, Malitson measured the refractive index of fused silica at various wavelengths at 20 °C and 30 °C [15]. The derived value for dn/dT of about 10 $\times 10^{-6}$ /K at 633 nm is close to our value of (9.7 $\pm$ 0.2) $\times 10^{-6}$ /K at 25 °C. Toyoda and Yabe also used the prism method and measured the refractive index at various wavelengths, from room temperature to 400 °C [35]. Their dn/dT value can thus be assigned to the average of the two temperature extremes, i.e. 210 °C. Extrapolating our polynomial for dn/dT to 210 °C we come up with a value of 12.4 $\times 10^{-6}$ /K, which is close to their reported average value of almost 12.7 $\times 10^{-6}$ /K. More recent studies report smaller values for dn/dT. The publication of Dupouy et al. sums up some recent results and presents their own interferometric data [18]. They calculated dn/dT from their measurements by using a value for the coefficient of thermal expansion which they obtained via private communication. They reported a single value of (9.18 $\pm$ 0.18) $\times 10^{-6}$ /K at 47.5 °C, which is near the middle of their temperature range. Our value of (10.1 $\pm$ 0.2) $\times 10^{-6}$ /K for this temperature is 9% higher. This deviation can be attributed to the different methods and the different synthesis of the fused silica samples.

Table 2 presents our value for α and values for dn/dT at a few discrete temperatures obtained from our measurement and calculated by Eq. (10). dn/dT increases about 10% from 20 °C to 80 °C. The reported standard deviation for dn/dT is derived from the standard deviation of γ, which was directly measured. The value for dn/dT was calculated using Eq. (6). For the error analysis, we refer the reader to the Appendix.

Table 2: The measured values of α and dn/dT for fused silica. For each temperature, the mean value of the experiments is given together with their standard deviation (*SD*). All values are in 10^{-6} /K. The error is estimated to be $\pm$ 0.04 $\times 10^{-6}$ /K for α and $\pm$ 0.2 $\times 10^{-6}$ /K for dn/dT.

	α	***dn/dT***						
	20 °C ... 80 °C	**20 °C**	**30 °C**	**40 °C**	**50 °C**	**60 °C**	**70 °C**	**80 °C**
Mean	0.64	9.65	9.79	9.94	10.09	10.24	10.38	10.53
SD	0.05	0.07	0.06	0.05	0.05	0.05	0.05	0.06

3.2. Pr:YLF

Pr:YLF has a coefficient of thermal expansion almost 20 times larger than fused silica. Therefore, the substrate interferometer showed about 16 fringes and we could use the approximate Eq. (2). The crystal interferometer showed from 14 to 16 fringes, depending on the crystallographic axis.

The reported results are the mean values of 27 experiments for α, 12 experiments for dn_o/dT for light polarized parallel to the a-axis (ordinary ray) and 21 experiments for dn_{eo}/dT for light

#220410 - $15.00 USD Received 4 Aug 2014; revised 7 Nov 2014; accepted 10 Nov 2014; published 3 Dec 2014

polarized parallel to the c-axis (extraordinary ray).

The polynomial for α for the a-axis obtained from the measurements is:

$$\alpha_{\mathrm{a}}(T) = 0.0236 \times 10^{-6}\,\mathrm{K}^{-2} \cdot T \; + \; 9.4487 \times 10^{-6}\,\mathrm{K}^{-1} \; , \tag{11}$$

where T should be in K. The polynomial is valid for the temperature range from 20 °C to 80 °C. The error was estimated to be $\pm\, 0.2 \times 10^{-6}$ /K (see Appendix).

Measured values for α of Pr:YLF crystals have not yet been reported. At least for the small dopant density of our crystal, it is expected that it is similar to those of YLF or (low-doped) Nd:YLF crystals. Koechner [8] and Bass [9] present data for Nd:YLF and YLF respectively without quoting any source. Their value of 13.3×10^{-6} /K for the a-axis corresponds to a temperature of about -110 °C for the polynomial presented by our study. We consider it highly probable that the value of 13.3×10^{-6} /K was indeed measured at a cryogenic temperature. Aggarwal et al. [13] investigated YLF in the temperature range from 80 K to 300 K, which just reaches the lower limit of our temperature range. They used a double Michelson laser interferometer and reported a value of 14.31×10^{-6} /K for α for the a-axis of YLF at 27 °C, averaged over four temperature cycles. At this temperature, our value of $(16.5 \pm 0.2) \times 10^{-6}$ /K, averaged over 27 temperature cycles, is 15% larger. Figure 6(a) presents our polynomial plotted together with the polynomial by Aggarwal et al.

Using Eqs. (7) and (8), the polynomials for dn_o/dT and dn_{eo}/dT are:

$$\frac{dn_o}{dT}(T) = -0.0169 \times 10^{-6}\,\mathrm{K}^{-2} \cdot T \; - \; 0.2569 \times 10^{-6}\,\mathrm{K}^{-1} \; , \tag{12}$$

$$\frac{dn_{eo}}{dT}(T) = -0.0161 \times 10^{-6}\,\mathrm{K}^{-2} \cdot T \; - \; 2.8970 \times 10^{-6}\,\mathrm{K}^{-1} \; , \tag{13}$$

where T should be in K. The polynomials are valid for the temperature range from 20 °C to 80 °C and for a wavelength of 633 nm. The error was estimated to be $\pm\, 0.3 \times 10^{-6}$ /K (see Appendix).

As in the case of α, no measured values for dn/dT of Pr:YLF have been reported and we can only compare our results with the values for undoped YLF or Nd:YLF crystals. We already mentioned that the majority of the published data for dn/dT of YLF and Nd:YLF go back to the same publication from 1980, when Barnes and Gettemy [12] used the prism method to measure the absolute refractive index of undoped YLF at three wavelengths, at room temperature and at liquid-nitrogen temperature. At a wavelength of 578 nm, which is the closest to our wavelength of 633 nm, they reported values of -0.91×10^{-6} /K for the ordinary refractive index and -2.86×10^{-6} /K for the extraordinary refractive index. These values can be assigned to the average of the two temperatures at which n was measured, i.e. about -90 °C as shown in Fig. 6(b), and are not directly comparable with our results, because of the different wavelengths and temperatures.

Pollak et al. quoted -0.8×10^{-6} /K for the ordinary refractive index and -3.0×10^{-6} /K for the extraordinary refractive index of YLF at a wavelength of 442 nm [36]. Later, the group of Pollak et al. quoted -2.0×10^{-6} /K for the ordinary refractive index and -4.3×10^{-6} /K for the extraordinary refractive index of Nd:YLF at a wavelength of 1064 nm [37]. Both publications refer to results of measurements given by private communications and provide no information about the temperature. Payne et al. quoted the latter values for YLF, without reference to the wavelength or the temperature [38].

Finally, Aggarwal et al. interferometrically measured γ for light polarized parallel to the a-axis and to the c-axis of YLF at 1064 nm [13]. Out of these data, they calculated dn/dT for the ordinary and the extraordinary axis in the temperature range from 80 K to 300 K. Their results

#220410 - $15.00 USD Received 4 Aug 2014; revised 7 Nov 2014; accepted 10 Nov 2014; published 3 Dec 2014

are not directly comparable to ours because of the different wavelength, but show the same tendency (decrease of dn/dT for both axes with increasing temperature) and have a similar difference between the two axes. Our polynomials for dn_o/dT and dn_{eo}/dT are plotted together with the polynomials by Aggarwal et al. in Fig. 6(b).

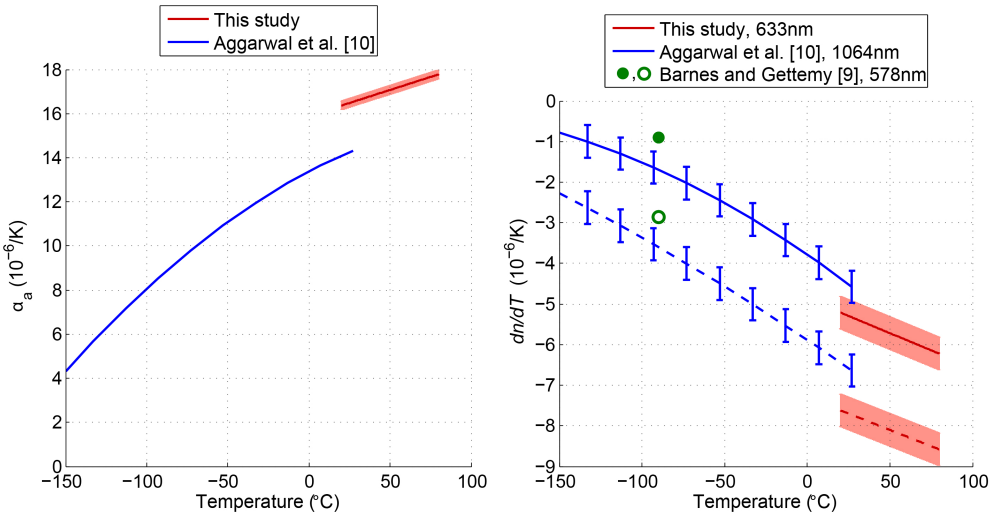

Fig. 6. (a): Our polynomial for α_a of Pr:YLF plotted together with the result of Aggarwal et al. for YLF [13]. Our error estimation of $\pm$ 0.2 $\times 10^{-6}$ /K is designated as a highlighted region around our result, because we have continuous data. Aggarwal et al. reported an error of $\pm$ 0.1 $\times 10^{-6}$ /K below 200 K and somewhat larger at higher temperatures.
(b): Our polynomials for dn/dT of Pr:YLF at 633 nm plotted together with the results of Barnes and Gettemy for YLF at 578 nm [12] and Aggarwal et al. also for YLF at 1064 nm [13]. The solid lines and the filled circle represent the ordinary refractive index, whereas the dashed lines and the blank circle represent the extraordinary refractive index. Our error estimation of $\pm$ 0.3 $\times 10^{-6}$ /K is designated as a highlighted region around our result, because we have continuous data. The (discrete) error bars for Aggarwal et al. correspond to their reported error of $\pm$ 0.4 $\times 10^{-6}$ /K.

dn/dT depends on both the temperature and the wavelength. From our results and the cited literature it is not clear whether dn/dT of Pr:YLF should be a monotonic function of the wavelength. The study of Barnes and Gettemy at three different wavelengths (435.8 nm, 546.1 nm and 578.0 nm) shows a tendency of dn/dT of undoped YLF to decrease with increasing wavelength for both axes at a cryogenic temperature [12]. It is not clear to us whether this tendency should also be expected for Pr:YLF at longer wavelengths and room temperature.

Table 3 presents the values for α and dn/dT at a few discrete temperatures obtained from our measurement and calculated using the polynomials of Eqs. (11)–(13). α increases by 9% and the absolute value of dn/dT increases by about 20% for the ordinary axis and 13% for the extraordinary axis from 20 °C to 80 °C. dn/dT for both axes is negative over the whole temperature range, with a larger absolute value for the extraordinary axis. The reported standard deviation for dn/dT is derived from the standard deviation of γ, which was directly measured. The values for dn/dT were calculated using Eqs. (7) and (8). For the error analysis, we refer the reader to the Appendix.

#220410 - $15.00 USD Received 4 Aug 2014; revised 7 Nov 2014; accepted 10 Nov 2014; published 3 Dec 2014

Table 3: The measured values of α and dn/dT for the Pr:YLF crystal. For each temperature, the mean value of the experiments is given together with their standard deviation (*SD*). All values are in 10^{-6}/K. The error is estimated to be $\pm$ 0.2 $\times 10^{-6}$/K for α and $\pm$ 0.3 $\times 10^{-6}$/K for dn/dT.

		20 °C	**30 °C**	**40 °C**	**50 °C**	**60 °C**	**70 °C**	**80 °C**
α_a	***Mean***	16.37	16.60	16.84	17.08	17.31	17.55	17.79
	SD	0.23	0.18	0.14	0.11	0.10	0.13	0.17
dn_o/dT	***Mean***	−5.21	−5.38	−5.55	−5.72	−5.89	−6.06	−6.23
	SD	0.10	0.08	0.06	0.05	0.04	0.05	0.07
dn_{eo}/dT	***Mean***	−7.62	−7.78	−7.94	−8.10	−8.26	−8.42	−8.58
	SD	0.13	0.10	0.09	0.08	0.08	0.10	0.12

4. Conclusions

We reported a phase-sensitive evaluation of simultaneous interferometric measurements of thermal expansion and thermal change of the refractive index of fused silica and Pr:YLF. Our method gives very reproducible results. The relative standard deviation of repeated measurements is below 1.5% for α and dn/dT of Pr:YLF (see Table 3).

We have chosen fused silica as a reference because it is a fairly well-characterized material with a small coefficient of thermal expansion, thus providing a challenging test of our measurement method. The small thermal expansion resulted in a relative standard deviation of 7.8%, almost 5 times larger than for Pr:YLF. Our short, 12 mm-long, fused silica sample expands by less than 0.5 µm for our temperature change from 20 °C to 80 °C. Our result for α measured on this short sample deviates by 12% from the calibration data provided by the manufacturer [30], indicating that our phase measurement has an absolute accuracy of about $\lambda/10$.

To our knowledge this is the first publication reporting α and dn/dT of Pr:YLF. There is a difference of 15% for α between our values and published values for undoped YLF. The values for dn/dT differ by 13%, but can not be directly compared because different wavelengths were used.

Appendix: Error analysis

The refractive index of air

Our vacuum chamber has a residual initial pressure (typically 18 mbar - 20 mbar) and a pressure increase during the experiments, attributed to a leakage and the temperature increase. The small α of fused silica allowed us to investigate this influence by deliberately changing the pressure. The influence is in the order of the standard deviation of α of fused silica (0.05×10^{-6}/K) and can be neglected for the measurement of γ of fused silica and α and γ of Pr:YLF, whose third significant digit is already in the order of 0.1×10^{-6}/K.

Error estimation

The random error for each data set is calculated using the standard error of the mean (*SEM*), which is defined as:

$$SEM = \frac{SD_m}{\sqrt{NoE}} , \tag{14}$$

where SD_m is the maximum standard deviation of the measured values of α and γ, and NoE is the Number of Experiments. The random error for 99.7% confidence limits is then $\pm 3 \cdot SEM$.

#220410 - $15.00 USD Received 4 Aug 2014; revised 7 Nov 2014; accepted 10 Nov 2014; published 3 Dec 2014

The results for SEM and $3 \cdot SEM$ are presented in Table 4, where the data are rounded up to two significant digits. α of fused silica is at the lower limit of our measurement capability. Consequently, the partial agreement with the manufacturer data allows us to use its random error as an estimation for the systematic error of the setup. The measurement error given in the last row of Table 4 is the sum of the systematic and random error for each data set.

Table 4: The maximum standard deviation for each measured quantity and the measurement error. All values are in 10^{-6}/K.

	Fused silica		**Pr:YLF**		
	$\boldsymbol{\alpha}$	$\boldsymbol{\gamma}$	$\boldsymbol{\alpha_a}$	$\boldsymbol{\gamma_a}$	$\boldsymbol{\gamma_c}$
$\boldsymbol{SD_m}$	0.05	0.07	0.23	0.10	0.13
NoE	13	13	27	12	21
SEM	0.014	0.020	0.045	0.029	0.029
3·SEM	0.042	0.060	0.135	0.087	
Measurement Error	0.042	0.102	0.177	0.129	

An accuracy of 0.01 mm is assumed for the length of the interferometers (0.08% for the fused silica sample and 0.20% for the Pr:YLF crystal). The error for the used values of the laser wavelength and the refractive indices is negligible. The overall error estimation is reported in Table 5. This estimation originates from the above analysis, taking into account the error propagation from the measurement of α and γ to the evaluation of dn/dT, which leads to a larger absolute error for dn/dT. The errors are rounded to one significant digit.

Table 5: The error estimation for each sample and reported quantity. All values are in 10^{-6}/K.

	Fused silica		**Pr:YLF**	
	$\boldsymbol{\alpha}$	***dn/dT***	$\boldsymbol{\alpha_a}$	***dn/dT***
Total Measurement Error	0.04	0.2	0.2	0.3

Acknowledgments

The authors gratefully acknowledge numerous advice and support by current and former members of the group, in particular Christian Büdenbender and Christian Vorholt.